IEEE Access
Multidisciplinary ⋮ Rapid Review ⋮ Open Access Journal

Received January 26, 2021, accepted February 9, 2021, date of publication February 11, 2021, date of current version February 23, 2021.

Digital Object Identifier 10.1109/ACCESS.2021.3058844

Rank Constrained Precoding for the Downlink of mmWave Massive MIMO Hybrid Systems

JOSÉ P. GONZÁLEZ-COMA[1], (Member, IEEE), ÓSCAR FRESNEDO[2], (Member, IEEE), AND LUIS CASTEDO[2], (Senior Member, IEEE)

[1]Defense University Center, Spanish Naval Academy, 36920 Marín, Spain
[2]Department of Computer Engineering & CITIC Research Center, University of A Coruña, 15001 A Coruña, Spain

Corresponding author: Óscar Fresnedo (oscar.fresnedo@udc.es)

This work has been funded by the Xunta de Galicia (by grant ED431C 2020/15, and grant ED431G2019/01 to support the Centro de Investigación de Galicia "CITIC"), the Agencia Estatal de Investigación of Spain (by grants RED2018-102668-T and PID2019-104958RB-C42) and European Regional Development Fund (ERDF) of the EU (FEDER Galicia 2014-2020 & AEI/FEDER Programs, UE).

ABSTRACT The hybrid design of precoding schemes for millimeter-wave communications allows exploiting the gains by using large antenna array with an affordable hardware cost and power consumption. In this work, we present a novel design strategy based on limiting the rank of the fully digital solutions before their decomposition into the analog and digital baseband components. This rank constraint on the digital formulation leads to a joint precoding and scheduling scheme where the number of allocated streams is limited according to the hardware constraints. In this way, the proposed approach can significantly reduce the performance losses caused by the direct decomposition of the unconstrained digital precoders. The resulting rank-constrained problems for the considered scenario are not convex and difficult to sort out. However, we propose several algorithms to compute the rank-constrained digital solutions with the help of the uplink-downlink duality for the achievable sum-rate. The obtained results show that this strategy achieves considerably higher sum-rates regardless of the channel conditions or available hardware resources.

INDEX TERMS Hybrid transceiver, Massive MIMO, mmWave communications, rank-constrained optimization.

I. INTRODUCTION

The fifth generation of cellular communications (5G) has been developed to satisfy challenging requirements in terms of traffic data, ultra-low latency and high transmission rates. For this reason, one of the key technologies proposed for the development of the 5G standard is the use of millimeter-wave (mmWave) [1]–[4]. However, these communications present a large attenuation and path losses because of using small wavelength signals [5], [6]. These effects can be mitigated by combining mmWave transmissions with the use of large antenna arrays at both transmission and reception [7]. Unfortunately, conventional massive Multiple-Input and Multiple-Output (MIMO) schemes lead to an unaffordable hardware cost and power consumption, since one dedicated radio frequency (RF) chain operating at mmWave frequencies is necessary at each antenna [5], [8], [9].

An alternative approach consists of considering a hybrid architecture where the RF processing is performed considering a limited number of RF chains, while the diversity gains provided by the massive MIMO schemes are exploited with digital baseband processing [10]–[12]. There exist different alternatives for implementing the RF stage, such as the use of switches, phase shifters or lens [8], [13], as well as different connection structures [14]–[16].

In this work, we focus on massive MIMO hybrid mmWave systems where all the RF chains are connected to all the antennas. In this setup, two major approaches have been considered in the literature:

1) The hybrid precoders/combiners are specifically designed according to some performance metric. In this case, the RF vectors are usually chosen from a finite codebook, typically maximizing the Signal-to-Noise Ratio (SNR). Next, the baseband matrices are optimized to maximize the considered metric [17]–[21]. This strategy relies on the baseband precoders to cancel the interference and performs poorly in certain scenarios since the degrees of freedom available for removing the interference are limited [22].

The associate editor coordinating the review of this manuscript and approving it for publication was Bilal Khawaja.

2) An unconstrained digital solution is first computed, and then a factorization algorithm is proposed to design a hybrid precoder that approximates these solution while fulfilling the hardware constraints. In the literature, we can find a huge variety of approaches aiming at reducing the gap between the performance obtained with the digital solution and the one achieved using the corresponding hybrid scheme [15], [23]–[28]. Although these works address the factorization problem from different point of view, all of them aim at the minimization of the Frobenius norm for the difference between the unconstrained digital precoder and the hybrid approach.

In general, hybrid precoding provides suboptimal performance with respect to fully digital solutions due to the additional constraints imposed by the hardware restrictions. However, it was show in [29] that if the number of RF chains is twice the total number of allocated data streams, a hybrid precoding achieves the same performance as the fully digital solution. This condition can be fulfilled as long as the number of users is small. Nevertheless, the number of required RF chains is usually unaffordable for communication scenarios with a large number of users. This is because digital precoder designs serve as many users as possible to maximize the achievable sum-rate.

An alternative would be to incorporate an appropriate scheduling strategy to limit the number of users according to the hardware resources. However, traditional scheduling approaches focus on maximizing the system performance by selecting the best configuration of users at each time, but it does not impose limitations on the number of served users or allocated streams [30]–[32]. Moreover, these approaches generally assume single-antenna users and a purely digital design. Thus, they cannot be applied directly to MIMO hybrid architectures. An exception is the work in [33], where the number of RF chains is taken into account in the design of the hybrid precoder and the corresponding implicit scheduling. However, this approach presents some issues. First, it again assumes single-antenna receivers which leads to allocating one stream at most to each active user, thus limiting the achievable performance. The proposed algorithm starts from the unconstrained precoding solution and then reduces the number of served users by removing some of them sequentially until the hardware constraints are satisfied. This approach is suboptimal since the precoding design and the posterior scheduling are performed at separate stages. Finally, the digital baseband precoder is designed according to the Zero-Forcing criterion. As aforementioned, this solution is unfeasible for some scenarios [22].

In this work, we focus on the design of a joint hybrid precoding and scheduling scheme for the downlink of massive MIMO mmWave systems. In the proposed approach, we first formulate an optimization problem for obtaining a digital precoding matrix with the desired rank. Next, some factorization algorithm can be applied to decompose the rank-constrained digital precoder into its corresponding RF and baseband components. This approach allows mitigating the considerable performance losses of the traditional solutions, which directly factorizes the unconstrained digital precoder. This improvement is motivated by the limitation on the rank of the digital solution that restricts the the number of allocated streams, thus working as a scheduling operation. Hence, our approach leads to a joint scheduling and precoding design adequate for a hybrid decomposition. This fact eventually results in larger achievable sum-rates.

Most common approaches to solve general optimization problems including the non-convex rank constraint are not specially suitable for our scenario, e.g., alternating direction method of multipliers (ADMM) [34], [35] or approximations based on the nuclear norm [36], [37] present convergence issues, whereas iterative rank minimization (IRM) [38] follows a general formulation which does not exploit the properties of the formulated problem. Accordingly, we propose two algorithms to compute the joint scheduling and digital precoding solution.

Hence, the main contributions of this work can be summarized as:

- A novel approach for the design of hybrid precoders in the downlink of massive MIMO mmWave schemes is proposed. The incorporation of rank constraints in the precoder design also enables an effective scheduling for this scenario, thus considering the number of available RF chains. The resulting joint precoding and scheduling scheme is able to reduce the losses of the traditional approach based on directly factorizing unconstrained digital solutions.
- Two particular algorithms are proposed for efficiently computing the rank-constrained digital solutions. These algorithms aim at exploiting the structure of the resulting optimization problem for the considered scenario.

A. NOTATION

Bold lower-case and upper-case letters are used for vectors and matrices, respectively, while regular letters denote scalars. For a given matrix $\boldsymbol{A}$, $\boldsymbol{A}^T$ and $\boldsymbol{A}^{\mathrm{H}}$ represent its transpose and conjugate transpose, respectively, whereas $[\boldsymbol{A}]_{i,j}$ is the element in the i-th row and j-th column of matrix $\boldsymbol{A}$. The operator diag$(\cdot)$ constructs a diagonal matrix with the arguments in its main diagonal and $\|\boldsymbol{A}\|_{\mathrm{F}}$ represents the Frobenius norm of a matrix. The operator tr$(\cdot)$ computes the trace of the argument and $\mathbb{E}[x]$ is the expectation of the random variable x.

II. SYSTEM MODEL

Let us consider the downlink of a cellular system where a base station (BS) equipped with N_{T} transmit antennas aims at communicating to U non-cooperative mobile users (MU). Each MU has the same number of receive antennas, N_{R}, to acquire the symbols from the communication channel. As introduced, the hardware and consumption requirements for this setup significantly increases as the number of transmit

and receive antennas grows. For this reason, the number of RF chains at the BS is limited to L_{BS}. Nevertheless, our approach is valid for realistic scenarios where the number of potential users is significantly larger than the number of available RF chains. Let $N_{\mathrm{s},u}$ be the number of data streams that are independently and simultaneously sent to user $u \in \{1, 2, \ldots, U\}$. Hence, the total number of transmitted streams is $N_{\mathrm{s}} = \sum_{u=1}^{U} N_{\mathrm{s},u}$. Let $\boldsymbol{s}_u \in \mathbb{C}^{N_{\mathrm{s},u}}$ be the data vector for the u-th user, with $\boldsymbol{s}_u \sim \mathcal{N}_{\mathbb{C}}(\mathbf{0}, \mathbf{I}_{N_{\mathrm{s},u}})$ and $\mathbb{E}[\boldsymbol{s}_u \boldsymbol{s}_j^{\mathrm{H}}] = \mathbf{0}$ for $u \neq j$. These data streams are first preprocessed at the BS using an appropriate linear precoding scheme and then transmitted over the common channel. Therefore, the signal received at each MU can be expressed as

$$\boldsymbol{x}_u = \boldsymbol{H}_u \sum_{i=1}^{U} \boldsymbol{P}_i \boldsymbol{s}_i + \boldsymbol{n}_u, \tag{1}$$

where $\boldsymbol{H}_u \in \mathbb{C}^{N_{\mathrm{R}} \times N_{\mathrm{T}}}$ represents the MIMO channel matrix response for the u-th user, $\boldsymbol{P}_i \in \mathbb{C}^{N_{\mathrm{T}} \times N_{\mathrm{s},u}}$, $i \in \{1, 2, \ldots, U\}$, represents the users precoding matrices and $\boldsymbol{n}_u \sim \mathcal{N}_{\mathbb{C}}(\mathbf{0}, \sigma_n^2 \mathbf{I}_{N_{\mathrm{R}}})$ is the additive white Gaussian noise (AWGN) for the u-th user. We assume a sum-power constraint at transmission, i.e., $\sum_{i=1}^{U} \mathrm{tr}(\boldsymbol{P}_i \boldsymbol{P}_i^{\mathrm{H}}) \leq P_{\mathrm{tx}}$, and define the system SNR as $\eta = P_{\mathrm{tx}}/\sigma_n^2$.

The limitations imposed by the hardware at the BS can be circumvented by considering a hybrid design of the transmit precoders $\boldsymbol{P}_u$, $u \in \{1, 2, \ldots, U\}$, where this precoding operation is split into two different phases: a baseband one different for each user and a RF one common to all users. Hence, the precoder matrices can be computed as $\boldsymbol{P}_u = \boldsymbol{P}_{\mathrm{RF}} \boldsymbol{P}_{\mathrm{BB}}^u$, where $\boldsymbol{P}_{\mathrm{BB}}^u \in \mathbb{C}^{L_{\mathrm{BS}} \times N_{\mathrm{s},u}}$ is the baseband precoder for the u-th user and $\boldsymbol{P}_{\mathrm{RF}} \in \mathbb{C}^{N_{\mathrm{T}} \times L_{\mathrm{BS}}}$ the common RF precoder. Since the RF precoders are implemented using analog phase shifters, their entries are restricted to have constant modulus, i.e., $|[\boldsymbol{P}_{\mathrm{RF}}]_{i,j}|^2 = 1$, $\forall\, i, j$. According to this hybrid design, (1) is rewritten as

$$\boldsymbol{x}_u = \boldsymbol{H}_u \sum_{i=1}^{U} \boldsymbol{P}_{\mathrm{RF}} \boldsymbol{P}_{\mathrm{BB}}^i \boldsymbol{s}_i + \boldsymbol{n}_u. \tag{2}$$

We next assume that the downlink transmission uses superposition coding with successive interference cancellation. Therefore, assuming Gaussian signaling and optimal decoding, the system model in the downlink yields the following achievable sum-rate for the u-th user [15], [18], [19]

$$R_u^{\mathrm{DL}} = \log_2 \det \left(\mathbf{I}_{N_{\mathrm{s},u}} + \boldsymbol{P}_u^{\mathrm{H}} \boldsymbol{H}_u^{\mathrm{H}} \boldsymbol{Z}_u^{-1} \boldsymbol{H}_u \boldsymbol{P}_u \right), \tag{3}$$

with $\boldsymbol{Z}_u = \sum_{i>u}^{U} \boldsymbol{H}_u \boldsymbol{P}_i \boldsymbol{P}_i^{\mathrm{H}} \boldsymbol{H}_u^{\mathrm{H}} + \sigma_n^2 \mathbf{I}_{N_{\mathrm{R}}}$. Henceforth, for fixed ordering, the rate expression in (3) only depends on the transmit covariance matrices $\boldsymbol{Q}_u = \boldsymbol{P}_u \boldsymbol{P}_u^{\mathrm{H}}$.

Considering the described scenario, the objective of this work is to provide an efficient hybrid design of the transmit covariance matrices $\boldsymbol{Q}_u$, $u = \{1, 2, \ldots, U\}$, in order to maximize the achievable sum-rate for the described communication system. In particular, we present a novel approach based on restricting the rank of the digital solution to mitigate the impact of decomposing the precoders into their corresponding baseband and analog components.

A. CHANNEL MODEL

We consider the geometric channel model [23], [39]. The MIMO channel response for the u-th user is given by

$$\boldsymbol{H}_u = \sqrt{\frac{N_{\mathrm{T}} N_{\mathrm{R}}}{N_{\mathrm{p}}}} \sum_{l=1}^{N_{\mathrm{p}}} \alpha_{u,l} \boldsymbol{a}_{\mathrm{R}}(\phi_{u,l}) \boldsymbol{a}_{\mathrm{T}}^{\mathrm{H}}(\theta_{u,l}), \tag{4}$$

where N_{p} is the number of channel paths, $\alpha_{u,l} \sim \mathcal{N}_{\mathbb{C}}(0, 1)$ is the channel gain for the l-th path, and $\boldsymbol{a}_{\mathrm{R}}(\phi_{u,l})$ and $\boldsymbol{a}_{\mathrm{T}}(\theta_{u,l})$ are the steering vectors for the MU and the BS, respectively. For simplicity, we consider uniform linear arrays (ULAs) at both ends of the communication link but the proposed method directly applies to other array configurations. Thus, the transmit steering vector assuming inter-antenna distance equal to half of the wavelength and Angle of Departure (AoD) $\theta_{u,l}$ is

$$\boldsymbol{a}_{\mathrm{T}}(\theta_{u,l}) = [1, \mathrm{e}^{-\mathrm{j}\pi \sin\theta_{u,l}}, \ldots, \mathrm{e}^{-\mathrm{j}\pi \sin\theta_{u,l}(N_{\mathrm{T}}-1)}]^T. \tag{5}$$

At reception, the expression for $\boldsymbol{a}_{\mathrm{R}}(\phi_{u,l})$ with Angle of Arrival (AoA) $\phi_{u,l}$ is similar to that in (5) and omitted for brevity.

B. DOWNLINK-UPLINK DUALITY

The calculations of the optimal capacity region for the general MIMO Broadcast Channel (BC) and an arbitrary number of users is not a trivial problem because it is based on the use of dirty paper techniques and, consequently, it implies non-convex formulations. Nevertheless, [32] shows that the BC dirty paper region is exactly equal to the capacity region of the dual MIMO Multiple Access Channel (MAC) considering the same sum-power constraint in both scenarios. This duality between the downlink and the uplink is also satisfied when considering the achievable sum-rate metric. Hence, we can maximize the achievable sum-rate in the dual MAC in an affordable way, and then exploit this duality to determine the optimal transmit covariance matrices for the BC.

Let us now introduce the system model for the dual uplink considering channel reciprocity, i.e., $\boldsymbol{H}_u^{\mathrm{H}}$ is the channel response for the u-th user in the uplink. The individual achievable rates are given by [32]

$$R_u^{\mathrm{UL}} = \log_2 \det \left(\mathbf{I}_{N_{\mathrm{T}}} + \boldsymbol{\Psi}_u^{-1} \boldsymbol{H}_u^{\mathrm{H}} \boldsymbol{T}_u \boldsymbol{T}_u^{\mathrm{H}} \boldsymbol{H}_u \right), \tag{6}$$

with $\boldsymbol{\Psi}_u = \sum_{i<u}^{U} \boldsymbol{H}_i^{\mathrm{H}} \boldsymbol{T}_i \boldsymbol{T}_i^{\mathrm{H}} \boldsymbol{H}_i + \sigma_n^2 \mathbf{I}_{N_{\mathrm{T}}}$ the interference plus noise matrix. The matrices $\boldsymbol{T}_i$ correspond to the precoding schemes employed for the users in the dual uplink model. Therefore, the achievable sum-rate in the uplink reads as

$$\sum_{u=1}^{U} R_u^{\mathrm{UL}} = \sum_{u=1}^{U} \log_2 \det \left(\mathbf{I}_{N_{\mathrm{T}}} + \boldsymbol{\Psi}_u^{-1} \boldsymbol{H}_u^{\mathrm{H}} \boldsymbol{T}_u \boldsymbol{T}_u^{\mathrm{H}} \boldsymbol{H}_u \right).$$

Note that this function is concave on the transmit covariance matrices $\boldsymbol{S}_u = \boldsymbol{T}_u \boldsymbol{T}_u^{\mathrm{H}}$. Furthermore, it is bounded by

$$\sum_{u=1}^{U} R_u^{\mathrm{UL}} \leq \log_2 \det \left(\mathbf{I}_{N_{\mathrm{T}}} + \sum_{u=1}^{U} \boldsymbol{H}_u^{\mathrm{H}} \boldsymbol{S}_u \boldsymbol{H}_u \right). \tag{7}$$

In addition, according to the BC-MAC duality [32], we will determine the optimal transmit covariance matrices $\boldsymbol{S}_u$ in the dual uplink using the concave expression in (7), and obtain from $\boldsymbol{S}_u$ the corresponding transmit covariance matrices, $\boldsymbol{Q}_u$, in the downlink.

In particular, the BC-MAC duality establishes that $R_u^{\mathrm{UL}} = R_u^{\mathrm{DL}}, \forall u$, with $\sum_{u=1}^{U} \mathrm{tr}(\boldsymbol{Q}_u) \leq \sum_{u=1}^{U} \mathrm{tr}(\boldsymbol{S}_u)$, as long as the transmit covariance matrices satisfy the relationship $\boldsymbol{Q}_u = \boldsymbol{\Delta}_u \boldsymbol{S}_u \boldsymbol{\Delta}_u^{\mathrm{H}}$, where $\boldsymbol{\Delta}_u$ represents the matrices for the uplink-downlink conversion. By defining the matrices

$$\begin{aligned} \boldsymbol{A}_u &= \mathbf{I}_{N_{\mathrm{R}}} + \sum_{i=1}^{u-1} \boldsymbol{H}_u \boldsymbol{Q}_i \boldsymbol{H}_u^{\mathrm{H}}, \\ \boldsymbol{B}_u &= \mathbf{I}_{N_{\mathrm{T}}} + \sum_{i=u+1}^{U} \boldsymbol{H}_i^{\mathrm{H}} \boldsymbol{S}_i \boldsymbol{H}_i, \end{aligned} \tag{8}$$

the matrices for the uplink-downlink conversion read as

$$\boldsymbol{\Delta}_u = \boldsymbol{B}_u^{-1/2} \boldsymbol{F}_u \boldsymbol{G}_u^{\mathrm{H}} \boldsymbol{A}_u^{1/2}, \tag{9}$$

with the singular value decomposition (SVD) $\boldsymbol{F}_u \boldsymbol{\Sigma}_u \boldsymbol{G}_u^{\mathrm{H}} = \boldsymbol{B}_u^{-1/2} \boldsymbol{H}_u^{\mathrm{H}} \boldsymbol{A}_u^{-1/2}$, $\boldsymbol{F}_u \in \mathbb{C}^{N_{\mathrm{T}} \times N_{\mathrm{R}}}$, $\boldsymbol{\Sigma}_u \in \mathbb{C}^{N_{\mathrm{R}} \times N_{\mathrm{R}}}$ and $\boldsymbol{G}_u \in \mathbb{C}^{N_{\mathrm{R}} \times N_{\mathrm{R}}}$.

III. PROBLEM FORMULATION

As commented, since the objective is to maximize the achievable sum-rate in the downlink considering a sum power constraint, the problem formulation can be expressed as

$$\max_{\boldsymbol{P}_{\mathrm{d}}} \sum_{u=1}^{U} R_u^{\mathrm{DL}} \quad \text{s.t. } \|\boldsymbol{P}_{\mathrm{d}}\|_{\mathrm{F}}^2 \leq P_{\mathrm{tx}}, \tag{10}$$

where the individual rates for the downlink are given by (3). Note that the overall precoding matrix $\boldsymbol{P}_{\mathrm{d}}$ is introduced for simplicity and stacks the precoders corresponding to all users, i.e., $\boldsymbol{P}_{\mathrm{d}} = [\boldsymbol{P}_1, \boldsymbol{P}_2, \ldots, \boldsymbol{P}_U] \in \mathbb{C}^{N_{\mathrm{T}} \times N_{\mathrm{s}}}$.

The above equation corresponds to the traditional formulation for the digital design of the precoder matrices, i.e., without considering hybrid precoding. In our particular scenario, the above problem is transformed into

$$\begin{aligned} \max_{\boldsymbol{P}_{\mathrm{RF}}, \boldsymbol{P}_{\mathrm{BB}}} & \sum_{u=1}^{U} R_u^{\mathrm{DL}} \\ \text{s.t. } & \|\boldsymbol{P}_{\mathrm{RF}} \boldsymbol{P}_{\mathrm{BB}}\|_{\mathrm{F}}^2 \leq P_{\mathrm{tx}}, \\ & |[\boldsymbol{P}_{\mathrm{RF}}]_{i,j}| = 1, \quad \forall i, j, \end{aligned} \tag{11}$$

with the overall baseband precoding matrix $\boldsymbol{P}_{\mathrm{BB}} = [\boldsymbol{P}_{\mathrm{BB}}^1, \ldots, \boldsymbol{P}_{\mathrm{BB}}^U] \in \mathbb{C}^{N_{\mathrm{RF}} \times N_{\mathrm{s}}}$. This formulation requires to consider constant-modulus constraints in the entries of $\boldsymbol{P}_{\mathrm{RF}}$ due to the use of phase shifters in the implementation of the common analog RF precoder. Unfortunately, these constraints make the resulting problem very difficult to deal with.

Prior art considered two main approaches to overcome these restrictive constraints: 1) the problem is first solved without the analog restrictions and, next, the RF and baseband precoders are designed to approximate such solution; and 2) the problem (11) is directly solved for a given metric or setup, and the hybrid solution is rigid. However, these strategies are highly dependent on the structure of the digital precoding matrix $\boldsymbol{P}_{\mathrm{d}}$, leading to poor results in general in comparison with the optimal solutions obtained from (10). This performance loss is closely related to the fact that the unconstrained digital solutions have a much larger rank than the number of RF chains. Consequently, the decomposition of $\boldsymbol{P}_{\mathrm{d}}$ into its corresponding RF and baseband precoders produces inaccurate approximations since the structure of $\boldsymbol{P}_{\mathrm{d}}$ is disregarded.

In this work, we propose an approach based on restricting the rank of digital solution $\boldsymbol{P}_{\mathrm{d}}$ to mitigate the impact of the subsequent matrix factorization, required to deal with the constraints in (11). Thus, the digital precoders are initially computed with an appropriate rank –depending on the number of available RF chains– and the constrained-rank solutions are then decomposed to obtain the RF and baseband precoders in the hybrid design. The mathematical formulation for the design of $\boldsymbol{P}_{\mathrm{d}}$ is given by

$$\begin{aligned} \max_{\boldsymbol{P}_{\mathrm{d}}} & \sum_{u=1}^{U} R_u^{\mathrm{DL}} \\ \text{s.t. } & \|\boldsymbol{P}_{\mathrm{d}}\|_{\mathrm{F}}^2 \leq P_{\mathrm{tx}}, \ \mathrm{rank}(\boldsymbol{P}_{\mathrm{d}}) \leq \gamma L_{\mathrm{BS}}, \end{aligned} \tag{12}$$

where $\gamma \geq 1$ is a parameter to balance between the unconstrained digital solution and the extreme case where $\boldsymbol{P}_{\mathrm{d}}$ has the same rank as the number of RF chains. This parameter hence establishes a trade-off between the performance of the digital solution and the accuracy of the subsequent factorization operation. Another consequence of using (12) is that the number of streams N_{s} and, accordingly, the number of users U that can be served simultaneously is limited by $U \leq N_{\mathrm{s}} \leq \gamma L_{\mathrm{BS}}$. Thus, the proposed problem formulation jointly performs a scheduling strategy and a precoding design. This behavior is similar to that in [40], [41], where some users or streams are allocated with zero power to enhance the performance metric but, in this case, we explicitly define the maximum number of allocated streams according to the hardware constraints.

As observed, problem (11) can now be addressed as a two stage problem and avoid the involved restrictions on the RF precoders. First, we impose a maximum rank restriction on the digital precoding matrix which in turn determines the number of streams served. Thereby, the solutions obtained from (12) will be rank-constrained which ensures that the hybrid decomposition will provide more accurate results. Although the rank constraint is again non-convex, several approaches in the literature have been proposed to address this kind of optimization problems.

IV. PROPOSED ALGORITHMS

In this section, we propose three different algorithms to determine the rank-constrained solutions for the optimization problem (12).

A. LOW-RANK MATRIX APPROXIMATION (LRMA)

This simple and intuitive idea is based on the Eckart-Young theorem. It consists in finding the matrix of rank L_{BS} that minimizes the Frobenius norm of the difference with respect to the unconstrained solution. Recall that the Frobenius norm was proposed as an approximation to maximize the achievable rate [23]. Thus, the constrained-rank solution is obtained from the following optimization problem

$$\min_{\boldsymbol{P}_{\mathrm{d}}} \|\boldsymbol{P}^{*}-\boldsymbol{P}_{\mathrm{d}}\|_{\mathrm{F}}^{2} \quad \mathrm{rank}(\boldsymbol{P}_{\mathrm{d}}) \leq L_{\mathrm{BS}}, \tag{13}$$

where $\boldsymbol{P}^{*}$ represents the digital solution disregarding the rank constraint. Note that $\boldsymbol{P}^{*}$ can be obtained by following the approach in [32].

The low-rank approximation for the optimal digital precoding matrix $\boldsymbol{P}^{*}$ can be computed from the SVD of $\boldsymbol{P}^{*}=\boldsymbol{U}\boldsymbol{\Sigma}\boldsymbol{V}^{\mathrm{H}}$, where the values of the diagonal matrix $\boldsymbol{\Sigma}$ are ordered in decreasing order $\sigma_1 \geq \sigma_2 \geq \sigma_{N_{\mathrm{T}}} \geq 0$. In such a case, the low-rank approximation is given by $\boldsymbol{P}_{\mathrm{d}}=\boldsymbol{U}\boldsymbol{\Sigma}_{\mathrm{d}}\boldsymbol{V}^{\mathrm{H}}$, where $\boldsymbol{\Sigma}_{\mathrm{d}}$ is a diagonal matrix with elements $[\boldsymbol{\Sigma}_{\mathrm{d}}]_{i,i}=\sigma_i$ for $i \leq L_{\mathrm{BS}}$ and $[\boldsymbol{\Sigma}_{\mathrm{d}}]_{i,i}=0$ for $i > L_{\mathrm{BS}}$. Note that this precoding matrix will be the optimal solution for the above optimization problem (see [42]). The precoding matrix $\boldsymbol{P}_{\mathrm{d}}$ is afterwards normalized to satisfy the sum-power constraint with equality.

B. PROXIMAL GRADIENT ALGORITHM (PGA)

This method is based on approximating the rank constraint by the nuclear norm, which is its convex surrogate function. However, the cost function in (12) is also not convex, but we can apply the DL-UL duality explained in Section II-B to replace the cost function in (12) by the expression of the sum-rate for the dual uplink given by (7). In this case, the convex reformulation based on the nuclear norm can be written using the Lagrangian objective function

$$\begin{aligned}\min_{\boldsymbol{P}_{\mathrm{d}},\lambda\geq 0,\mu\geq 0} \; & \mu\|\boldsymbol{P}_{\mathrm{d}}\|_{*}+\lambda\left(\|\boldsymbol{P}_{\mathrm{d}}\|_{\mathrm{F}}^{2}-P_{\mathrm{tx}}\right) \\ & -\log_2\det\left(\mathbf{I}_{N_{\mathrm{T}}}+\sum_{u=1}^{U}\boldsymbol{H}_u^{\mathrm{H}}\boldsymbol{\Delta}_u\boldsymbol{P}_u\boldsymbol{P}_u^{\mathrm{H}}\boldsymbol{\Delta}_u^{\mathrm{H}}\boldsymbol{H}_u\right)\end{aligned} \tag{14}$$

with $\boldsymbol{P}_{\mathrm{d}}$ stacking the individual downlink precoders and $\boldsymbol{\Delta}_u$ being the matrices for the downlink to uplink conversion, which are considered given and fixed. This approximation does not establish an upper or a lower bound since a feasible solution for (14) may not satisfy the rank constraint.

To solve (14), we employ the proximal gradient method, which is commonly used to address non-smooth optimization problems, such as in matrix completion optimizations [43] or compressed sensing [44]. Let us split the objective function in (14) as the sum of the nuclear norm and the function $g(\boldsymbol{P}_{\mathrm{d}},\lambda)$, i.e., $\mu\|\boldsymbol{P}_{\mathrm{d}}\|_{*}+g(\boldsymbol{P}_{\mathrm{d}},\lambda)$, where

$$\begin{aligned}g(\boldsymbol{P}_{\mathrm{d}},\lambda) = & \lambda\left(\|\boldsymbol{P}_{\mathrm{d}}\|_{\mathrm{F}}^{2}-P_{\mathrm{tx}}\right) \\ & -\log_2\det\left(\mathbf{I}_{N_{\mathrm{T}}}+\sum_{u=1}^{U}\boldsymbol{H}_u^{\mathrm{H}}\boldsymbol{\Delta}_u\boldsymbol{P}_u\boldsymbol{P}_u^{\mathrm{H}}\boldsymbol{\Delta}_u^{\mathrm{H}}\boldsymbol{H}_u\right)\end{aligned} \tag{15}$$

Note that $g(\cdot)$ is differentiable on $\boldsymbol{P}_{\mathrm{d}}$. Thus, we can compute the gradient as

$$\nabla g(\boldsymbol{P}_{\mathrm{d}})=\left[\frac{\mathrm{d}g(\boldsymbol{P}_{\mathrm{d}},\lambda)}{\mathrm{d}\boldsymbol{P}_1^{*}},\ldots,\frac{\mathrm{d}g(\boldsymbol{P}_{\mathrm{d}},\lambda)}{\mathrm{d}\boldsymbol{P}_U^{*}}\right], \tag{16}$$

with $\frac{\mathrm{d}g(\boldsymbol{P}_{\mathrm{d}},\lambda)}{\mathrm{d}\boldsymbol{P}_u^{*}}$ provided in App. A. Contrary to $g(\cdot)$, the nuclear norm is not a smooth function. Fortunately, its subdifferential has been previously characterized as [45]

$$\partial\|\boldsymbol{X}\|_{*}=\boldsymbol{U}_{\boldsymbol{X}}\boldsymbol{V}_{\boldsymbol{X}}^{\mathrm{H}},$$

where $\boldsymbol{X}=\boldsymbol{U}_{\boldsymbol{X}}\boldsymbol{\Sigma}_{\boldsymbol{X}}\boldsymbol{V}_{\boldsymbol{X}}^{\mathrm{H}}$. According to the Karush-Kuhn-Tucker (KKT) conditions, $\boldsymbol{P}_{\mathrm{d}}^{\mathrm{opt}}$ is an optimum solution to (14) if and only if

$$\mu\partial\|\boldsymbol{P}_{\mathrm{d}}^{\mathrm{opt}}\|_{*}+\nabla g(\boldsymbol{P}_{\mathrm{d}}^{\mathrm{opt}})=\mathbf{0}. \tag{17}$$

In the following, we develop a fixed point algorithm similar to that in [45]. Considering a step size $s > 0$, the former expression can be rewritten as

$$s\mu\partial\|\boldsymbol{P}_{\mathrm{d}}^{\mathrm{opt}}\|_{*}-\boldsymbol{P}_{\mathrm{d}}^{\mathrm{opt}}+\bar{\boldsymbol{P}}_{\mathrm{d}}, \tag{18}$$

with the update $\bar{\boldsymbol{P}}_{\mathrm{d}}=\boldsymbol{P}_{\mathrm{d}}^{\mathrm{opt}}-s\nabla g(\boldsymbol{P}_{\mathrm{d}}^{\mathrm{opt}})$. Interestingly, this update is the optimal solution to the following problem

$$\min_{\boldsymbol{P}_{\mathrm{d}}} s\mu\|\boldsymbol{P}_{\mathrm{d}}\|_{*}+\|\boldsymbol{P}_{\mathrm{d}}-\bar{\boldsymbol{P}}_{\mathrm{d}}\|_{\mathrm{F}}^{2}. \tag{19}$$

Observe that the Frobenius norm appears again as the metric to determine the "closeness" to the unconstrained updates.

Finally, we define the matrix shrinkage operator (MSO) as

$$\Gamma_{s\mu}(\boldsymbol{X})=\boldsymbol{U}_{\boldsymbol{X}}\left(\boldsymbol{\Sigma}_{\boldsymbol{X}}-\boldsymbol{M}\right)\boldsymbol{V}_{\boldsymbol{X}}^{\mathrm{H}}, \tag{20}$$

where $\boldsymbol{X}=\boldsymbol{U}_{\boldsymbol{X}}\boldsymbol{\Sigma}_{\boldsymbol{X}}\boldsymbol{V}_{\boldsymbol{X}}^{\mathrm{H}}$ is a matrix of rank r, $\boldsymbol{M}=s\,\mathrm{diag}\left(\mu,\ldots,\mu,\frac{\sigma_d}{s},\ldots,\frac{\sigma_r}{s}\right)$, and the eigenvalues satisfy $\sigma_r \leq \ldots \leq \sigma_d \leq s\mu$. Hence, $\Gamma_{s\mu}(\bar{\boldsymbol{P}}_{\mathrm{d}})$ provides the optimal solution to (19) (see [45]). That is, the rank of the precoder matrix $\boldsymbol{P}_{\mathrm{d}}$ can be reduced from r to d by using the MSO in (20), although the resulting rank d is not known beforehand and depends on the parameter μ. This trade-off parameter has to be chosen empirically.

The proposed algorithm based on the proximal gradient is summarized in Table 1, and the proof of the convergence is relegated to App. B.

The main advantages of the proximal gradient approach are the following. It is flexible since we can substitute the achievable rate with another criterion. In addition, it presents a reasonable computational complexity. However, this algorithm presents a drawback. It is highly dependent on the starting point, as the proof of convergence leverages the use of approximately fixed DL-UL conversion matrices $\boldsymbol{\Delta}_u$ and optimum precoding directions. Then, similar to other steepest methods with locally optimum convergence, the initial step size s_{ini} must be carefully chosen to avoid divergences for certain initializations.

Algorithm 1 Proximal Gradient Algorithm (PGA)

Initialize: $\ell \leftarrow 0$, $\boldsymbol{P}_{\mathrm{d}}(0)$
repeat
  $f(\ell) = \mu\|\boldsymbol{P}_{\mathrm{d}}(\ell)\|_* + g(\boldsymbol{P}_{\mathrm{d}}(\ell), \lambda)$
  $\boldsymbol{\Delta}_u(\ell) \leftarrow$ Compute using (9) $\forall u$
  $\boldsymbol{G}_u(\ell) \leftarrow$ Determine as in (24)
  $\nabla g(\boldsymbol{P}_{\mathrm{d}}(\ell))$ Compute with (16), $s \leftarrow s_{\mathrm{ini}}, f(\ell+1) = 0$
  while $f(\ell) > f(\ell+1)$ **do**
    $\boldsymbol{P}_{\mathrm{cand}} = \boldsymbol{P}_{\mathrm{d}}(\ell) + s\nabla g(\boldsymbol{P}_{\mathrm{d}}(\ell))$
    $\boldsymbol{P}_{\mathrm{cand}} = \Gamma_{s\mu}(\boldsymbol{P}_{\mathrm{cand}})$
    $\boldsymbol{P}_{\mathrm{cand}} = \frac{\sqrt{P_{\mathrm{tx}}}}{\|\boldsymbol{P}_{\mathrm{cand}}\|_{\mathrm{F}}}\boldsymbol{P}_{\mathrm{cand}}$
    $f(\ell+1) = \mu\|\boldsymbol{P}_{\mathrm{cand}}\|_* + g(\boldsymbol{P}_{\mathrm{cand}}, \lambda)$
    $s = \frac{s}{2}$
  end while
  $\boldsymbol{P}_{\mathrm{d}}(\ell+1) = \boldsymbol{P}_{\mathrm{cand}}$
  $\ell \leftarrow \ell + 1$
until $\ell = L$

C. ITERATIVE TRACE ALGORITHM (ITA)

This method is based on replacing the rank constraint with a convex approximation and defining an iterative algorithm which solves the resulting convex optimization problems at each iteration. In this case, the alternative problem formulation is given by

$$\max_{\{\boldsymbol{S}_u\}_{u=1}^U} \log_2 \det(\mathbf{I}_{N_{\mathrm{T}}} + \sum_{u=1}^U \boldsymbol{H}_u^{\mathrm{H}}\boldsymbol{S}_u\boldsymbol{H}_u)$$
$$\text{s.t.} \sum_{u=1}^U \mathrm{tr}(\boldsymbol{S}_u) \leq P_{\mathrm{tx}}, \quad \sum_{u=1}^U t_u(\boldsymbol{S}_u, \bar{\boldsymbol{U}}, \boldsymbol{\Delta}_u) \leq \frac{P_{\mathrm{tx}}}{\alpha}, \quad (21)$$

where we introduce $t_u(\boldsymbol{S}_u, \bar{\boldsymbol{U}}, \boldsymbol{\Delta}_u) = \mathrm{tr}(\bar{\boldsymbol{U}}^{\mathrm{H}}\boldsymbol{\Delta}_u\boldsymbol{S}_u\boldsymbol{\Delta}_u^{\mathrm{H}}\bar{\boldsymbol{U}})$ and the downlink covariance matrix decomposition

$$\boldsymbol{Q} = \sum_{u=1}^U \boldsymbol{\Delta}_u\boldsymbol{S}_u\boldsymbol{\Delta}_u^{\mathrm{H}} = [\boldsymbol{U}\bar{\boldsymbol{U}}]\boldsymbol{\Sigma}[\boldsymbol{U}\bar{\boldsymbol{U}}]^{\mathrm{H}}, \quad (22)$$

with the basis $\boldsymbol{U} \in \mathbb{C}^{N_{\mathrm{T}} \times L_{\mathrm{BS}}}$, and $\bar{\boldsymbol{U}} \in \mathbb{C}^{N_{\mathrm{T}} \times N_{\mathrm{T}} - L_{\mathrm{BS}}}$.

As observed, the proposed convex relaxation limits the amount of transmit power leaked to the subspace of dimension $N_{\mathrm{T}} - L_{\mathrm{BS}}$ spanned by the basis $\bar{\boldsymbol{U}}$. The parameter α is again considered to establish a trade-off between rank-limitation and high-performance solutions. Indeed, on the one hand, the trace constraint is equivalent to a rank limitation when $\alpha \to \infty$ while, on the other, we obtain the unconstrained uplink digital problem formulation when $\alpha = 1$.

Using the convex relaxation in (21) we propose an algorithmic solution to design covariance matrices satisfying the rank constraint. Algorithm 2 summarizes the steps of the proposed algorithm based on the trace constraint. At each iteration ℓ, the algorithm updates the matrices $\{\boldsymbol{\Delta}_u(\ell)\}_{u=1}^U$ by using the uplink-downlink duality, and computes the matrices $\bar{\boldsymbol{U}}(\ell)$ by applying the eigen-decomposition in (22) to the uplink covariance matrices obtained in the previous iteration, i.e., $\{\boldsymbol{S}_u(\ell)\}_{u=1}^U$. Next, (21) is solved with a semi-definite program solver to update the uplink covariance matrices, i.e, $\{\boldsymbol{S}_u(\ell+1)\}_{u=1}^U$. Finally, the parameter $\alpha(\ell)$ is appropriately updated.

Algorithm 2 Iterative Trace Algorithm (ITA)

Initialize: $\ell \leftarrow 0$, $\alpha(0) \leftarrow \alpha_0$, $\{\boldsymbol{S}_u(0)\}_{u=1}^U$
repeat
  $\boldsymbol{\Delta}_u(\ell) \leftarrow$ Compute using (9) $\forall u$
  $\boldsymbol{Q}(\ell) = \sum_{u=1}^U \boldsymbol{\Delta}_u(\ell)\boldsymbol{S}_u(\ell)\boldsymbol{\Delta}_u(\ell)^{\mathrm{H}}$
  $\bar{\boldsymbol{U}}(\ell) \leftarrow$ Calculate with (22)
  $\{\boldsymbol{S}_u(\ell+1)\}_{u=1}^U \leftarrow$ Solve convex problem in (21)
  $\alpha(\ell+1) = \beta(\ell)\alpha(\ell)$
  $\ell \leftarrow \ell + 1$
until $\ell = L$

Besides its intuitive nature, this algorithm also presents good convergence properties under mild conditions. In particular, it is required to assume that the matrices to perform the DL-UL conversion slowly vary in successive iterations, i.e., $\boldsymbol{\Delta}_u(\ell+1) \approx \boldsymbol{\Delta}_u(\ell)$. Due to the iterative computation of the matrices $\boldsymbol{\Delta}_u$, this condition is difficult to show theoretically. However, we have experimentally verified that this assumption holds in the considered scenarios. The proof is provided in App. C.

D. ANALYSIS OF THE COMPUTATIONAL COMPLEXITY

In this section, we briefly analyze the computational complexity of the three previously proposed algorithms. Table 1 shows the operation with the highest computational cost for each algorithm and its corresponding complexity order. Thus, the overall computational complexity of the algorithms will be dominated by the operations in the table.

TABLE 1. Computational Complexity of the Different Algorithms.

Algorithm	Operation	Complexity
ITA	Compute solution for SDP problem in (21) [step 6]	$\mathcal{O}\left(N_{\mathrm{T}}^6\right)$
PGA	Update gradient [step 6]	$\mathcal{O}\left(N_{\mathrm{T}}^3\right)$
LRMA	Compute svd of the matrix $\boldsymbol{P}^*$	$\mathcal{O}\left(N_{\mathrm{T}}N_{\mathrm{R}}^2\right)$

Unlike the LRMA-based approach, ITA and PGA are iterative methods and, therefore, the computational cost is influenced by the number of iterations required to reach convergence. In practice, we have checked that this number of iterations is relatively small (about 10 iterations) which means to incorporate a linear factor whose impact vanishes as the number of transmit antennas grows.

As observed, the ITA approach has a complexity order significantly higher than that of the other two algorithms. This is because general-purpose solvers for semidefinite programming (SDP) problems are based on interior point methods whose computational time complexity has an order of $\mathcal{O}(mn^2+n^3)$ for a SDP problem with m linear matrix inequalities and n variables [46], [47]. PGA and LRMA present a lower complexity order since it is mostly determined by a matrix inversion and an SVD operation, respectively.

V. SIMULATION RESULTS

In this section, we present the results obtained in different computer simulations carried out to evaluate the performance of the proposed approach and the different optimization algorithms.

We consider a downlink setup with a BS equipped with $N_{\mathrm{T}} = 32$ antennas and $U = 10$ users with $N_{\mathrm{R}} = 2$ receive antennas each. Unless otherwise stated, we also assume that the number of available RF chains at the BS is $L_{\mathrm{BS}} = 4$. The precoded signals are transmitted to the users assuming a mmWave communication channel and ULAs at the BS and MUs as explained in Section II-A. Recall that an important parameter determining the channel behavior is the number of paths N_{p}. Finally, the performance of the different schemes is determined by averaging the achievable sum-rates obtained over 200 channel realizations in each experiment.

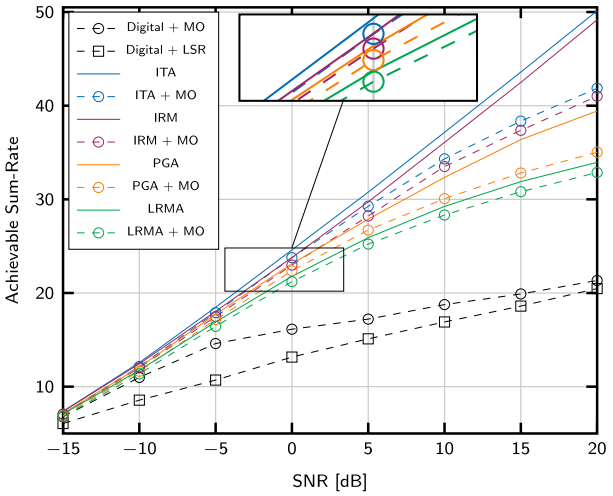

FIGURE 1. Performance comparison between several algorithms for a downlink with $N_{\mathrm{T}} = 32$ antennas, $N_{\mathrm{R}} = 2$ antennas, $U = 10$ users, $L_{\mathrm{BS}} = 4$ RF chains and $N_{\mathrm{p}} = 4$ channel paths. The curves corresponding to the hybrid schemes are obtained from a factorization of the digital solutions with the MO approach.

Figure 1 shows the sum-rates obtained for several strategies to design the BS precoder in the described downlink setup and considering $N_{\mathrm{p}} = 4$ paths. In particular, the performance of the following design strategies is compared: 1) ITA algorithm; 2) Iterative rank minimization (IRM) algorithm [38]; 3) PGA algorithm; and 4) LRMA. Thus, the three approaches proposed in this article to obtain the digital constrained-rank precoders are also compared to a well-known algorithm employed to solve optimization problems with rank constraints. As observed, the ITA-based strategy provides the best results in terms of achievable sum-rate for all the range of considered SNRs. This strategy is able to provide a constant gain with respect to the IRM algorithm with a similar computational cost. The PGA-based approach exhibits similar performance to the former strategies for low and medium SNRs, but it shows certain degradation for high SNR values, although its computational complexity is quite lower. Finally, LRMA presents the worst performance, but its computational cost is negligible. Therefore, the choice of one or other strategy will depend on the application trade-off between complexity and performance.

The aforementioned strategies provide the digital rank-constrained precoders for each channel realization. However, the advantage of limiting the rank of the digital precoders is to mitigate the impact of the decomposition required to obtain the hybrid solutions. The loss caused by the factorization of the different rank-constrained solutions is also shown in Figure 1. The achievable sum-rates obtained from the direct factorization of the optimal digital solution, i.e., without rank limitation, are also included to show the advantages of incorporating the rank constraint in the design of the digital precoders. Recall that these traditional approaches optimize the precoding matrices by performing a user scheduling which maximizes the sum-rate, but they are not able to limit the effective number of allocated streams. We consider two widely employed factorization algorithms in the context of hybrid precoding: least square relaxation (LSR) [24] and alternating minimization based on manifold optimization (MO) [15]. On the one hand, it is possible to appreciate that MO-based factorization provides better performance than LSR. On the other hand, both strategies exhibit a certain degree of saturation as SNR increases, which is still present for rank-constrained solutions. However, the most relevant conclusion is that the limitation on the rank of the digital precoders significantly mitigates the loss due to the factorization operation and leads to much larger sum-rates in a hybrid architecture. Other factorization algorithms have also been assessed, but they do not improve the performance of MO-based factorization.

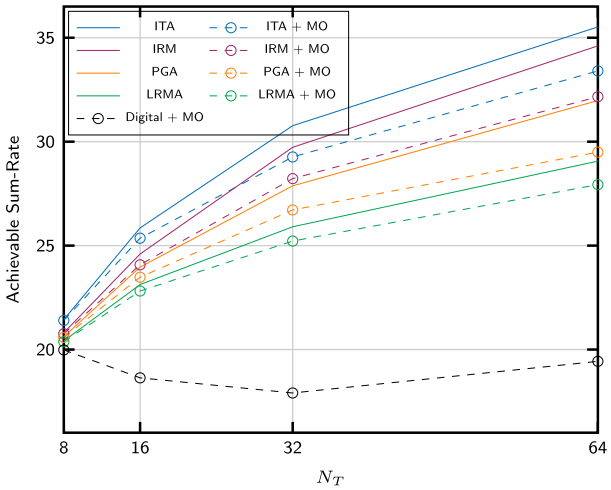

FIGURE 2. Comparison between the proposed algorithms for a downlink with $N_{\mathrm{T}} = \{8, 16, 32, 64\}$ antennas, $N_{\mathrm{R}} = 2$ antennas, $U = 10$ users, $L_{\mathrm{BS}} = 4$ RF chains, and considering $N_{\mathrm{p}} = 4$ propagation paths and a SNR value of 5dB. The curves corresponding to the hybrid schemes are obtained with the MO-based approach.

Figure 2 shows the impact of considering a different number of antennas for a fixed SNR value of 5dB in the same scenario as in the previous experiment. We can observe that

TABLE 2. Performance Losses Due to the Factorization of the Digital Precoders Obtained With Different Strategies and Different Numbers of Channel Paths.

SNRs	-10 dB			0 dB			10 dB			20 dB		
Alg. \ N_p	1	4	8	1	4	8	1	4	8	1	4	8
Digital	2.16	2.63	3.29	11.28	13.52	14.86	28.08	37.91	39.97	50.31	63.83	67.59
ITA	0.01	0.39	0.67	0.04	0.75	0.82	0.21	2.32	2.69	1.24	6.62	8.11
IRM	0.02	0.41	0.59	0.04	0.74	0.83	0.21	2.29	2.74	1.03	7.19	8.42
PGA	0.01	0.43	0.55	0.02	0.69	0.73	0.08	1.96	2.05	1.08	4.03	4.48
LRMA	0.01	0.37	0.52	0.02	0.48	0.59	0.05	0.72	0.79	0.05	0.84	0.98

TABLE 3. Factorization Losses for Different Number of RF Chains.

SNRs	0 dB				20 dB			
Alg. \ L_{BS}	2	4	6	8	2	4	6	8
Digital	29.91	20.91	12.42	3.96	86.22	79.71	70.5	58.3
ITA	0.49	0.76	0.65	0.45	3.03	7.43	7.04	6.16
IRM	0.52	0.77	0.75	0.46	3.11	7.79	7.39	6.49
PGA	0.39	0.76	0.61	0.45	1.98	4.40	5.76	6.09
LRMA	0.34	0.56	0.54	0.44	0.32	1.12	1.9	3.42

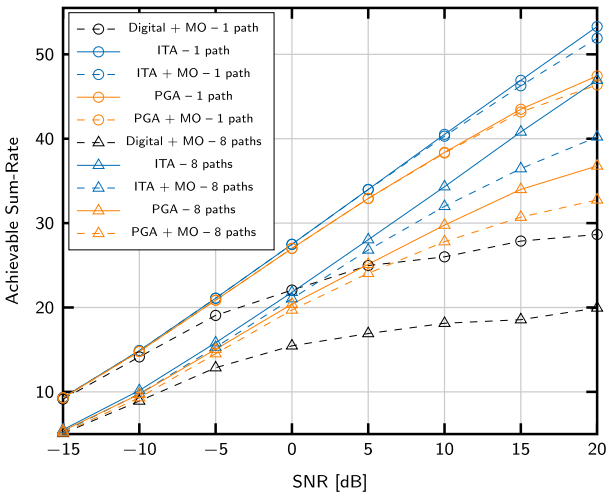

FIGURE 3. Comparison between the proposed algorithms for a downlink with $N_T = 32$ antennas, $N_R = 2$ antennas, $U = 10$ users, $L_{BS} = 4$ RF chains and considering $N_p = 1$ and $N_p = 8$ paths. The curves corresponding to the hybrid schemes are obtained with the MO-based approach.

the conclusions extracted from the results obtained in the previous experiment also apply when we modify the number of antennas. Thus, the low-rank digital precoding designs provide a superior performance when they are employed to compute their hybrid components. Indeed, the performance gains provided by the proposed approach increase with the number of antennas as this reduces the amount of user interference and, as a consequence, the number of allocated streams for an unconstrained digital design. Moreover, the advantage of utilizing the methods ITA and PGA, with respect to LRMA, also presents a similar behavior.

In the next experiment, we focus on analyzing the impact of the number of channel paths on the factorization losses with the proposed low-rank digital precoder designs. Figure 3 and Table 2 present the obtained results for the predetermined setup considering two options for the number of channel paths, $N_p = 1$ and $N_p = 8$. According to these results, it is worth highlighting two main conclusions. First, the loss due to the factorization is larger as the number of channel paths increases, regardless of the considered approach. This result was expected since a larger number of paths implies a higher channel diversity and, consequently, a further challenge to exploit this diversity with a hybrid architecture. Second, the approaches based on limiting the rank of the digital precoders before applying the factorization operation significantly mitigates the corresponding performance loss. Obviously, this improvement is achieved at the expense of penalizing the performance of the considered low-rank digital solution compared to the unconstrained one. However, this strategy is preferable for the design of the hybrid precoders at the BS as it provides better performance in terms of achievable sum-rate (see Figure 3).

Another interesting remark is the fact that although LRMA or PGA approaches present a higher resilience to factorization losses, its overall performance (rank-constrained solutions + factorization) is inferior to the other two constraining strategies. This is mostly motivated because the performance gap between the rank-constrained algorithms also increases as the number of channel paths is larger. Finally, the achievable sum-rates decrease with the number of channel paths. This behavior can be explained from the considered channel model in (4), where the channel gains are normalized

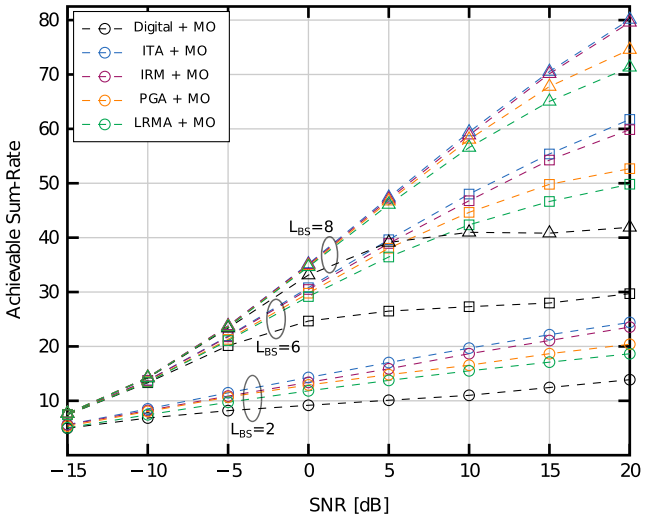

FIGURE 4. Comparison between the different algorithms for a downlink with $N_T = 32$ antennas, $N_R = 2$ antennas, $U = 10$ users, $N_p = 4$ channel paths and considering different number of RF chains. In particular, the triangle markers correspond to the performance curves obtained for $L_{BS} = 8$ chains, the square markers for $L_{BS} = 6$ chains and the circle markers for $L_{BS} = 2$ chains. In addition, the same color is employed to identify the same method through the different scenarios. Finally, the curves for the hybrid schemes are obtained with the MO-based factorization.

by the number of paths, N_p. Therefore, when the number of channel paths is larger than the number of streams allocated to each user, increasing the number of paths actually implies transmitting the same streams over paths with lower power. Recall that the number of allocated streams is limited by the constraint on the number of RF chains.

Finally, we evaluate the impact of the number of considered RF chains on the performance of the proposed algorithms. Figure 4 shows the achievable sum-rate obtained for the different hybrid precoding schemes after the factorization operation with the MO algorithm. We considered the setup described at the beginning of this section with $N_p = 4$ channel paths and three different configurations for the number of available RF chains: $L_{BS} = 2$, $L_{BS} = 6$ and $L_{BS} = 8$. For the same scenario, Table 3 shows the factorization losses for the different schemes and for two particular SNR values. As observed, these results are consistent with those obtained in previous experiments. Thus, the largest sum-rate is always provided by the ITA-based hybrid scheme, whereas the LRMA-based one achieves the worst performance even though the factorization loss is lower than in the other alternatives.

As expected, the sum-rate of the all considered schemes increases with the number of RF chains since the hardware constraints are less restrictive and a larger number of streams can be allocated. In addition, the gains provided by the rank-constrained approaches with respect to the direct factorization of the unconstrained solution are also more remarkable for larger values of L_{BS}. However, it is interesting to note that the factorization losses tend to decrease for ITA and IRM strategies as the number of RF chains is larger (from $L_{BS} > 2$), whereas this loss always increases with the number of RF chains for the PGA and LRMA approaches. These results suggest that the structure of the high-rank solutions provided by these two latter strategies is less suitable for their posterior factorization step.

VI. CONCLUSION

In this work, the design of practical low-computational hybrid precoding schemes has been addressed for massive MIMO mmWave communication systems. Instead of factorizing the optimal unconstrained digital solutions, we have proposed to limit the rank of such digital solutions prior to be factorized. The incorporation of this additional constraint allows accommodating the structure of the obtained solutions to the factorization operation and significantly mitigate the corresponding factorization loss. Hence, the proposed design represents a novel approach to jointly perform precoding and scheduling, thus limiting the number of allocated streams in a massive MIMO hybrid scenario.

In addition, two particular algorithms have been proposed to tackle the resulting rank-constrained problems. On the one hand, ITA provides the best performance in terms of achievable sum-rate, whereas PGA shows a certain loss with respect to ITA, but its computational cost is significantly lower. The obtained results clearly show the suitability of the proposed design for hybrid architectures since it provides much better results than the previous strategies.

Future research lines include more complex scenarios, e.g., the wideband case. Moreover, it is desirable to perform a theoretical analysis to lower the computational costs, avoid convergence dependencies on UL-DL conversion matrices, and refine the factorization method according to our digital design.

APPENDIX A
PGA GRADIENT

In this section we determine the gradient of $g(\boldsymbol{P}_d, \lambda)$ in (15). For convenience, we focus on the i-th precoder and rewrite $g(\boldsymbol{P}_d, \lambda)$ as follows

$$\begin{aligned} g(\boldsymbol{P}_d, \lambda) = \lambda &\left(\sum_{u=1}^{U} \|\boldsymbol{P}_u\|_F^2 - P_{tx} \right) \\ &- \log_2 \det \left(\mathbf{I}_{N_T} + \boldsymbol{G}_i^H \boldsymbol{P}_i \boldsymbol{P}_i^H \boldsymbol{G}_i \right) \\ &- \log_2 \det \left(\mathbf{I}_{N_T} + \sum_{u \neq i} \boldsymbol{H}_u^H \boldsymbol{\Delta}_u \boldsymbol{P}_u \boldsymbol{P}_u^H \boldsymbol{\Delta}_u^H \boldsymbol{H}_u \right), \end{aligned} \tag{23}$$

with $\lambda \geq 0$ the dual variable corresponding to the power constraint and

$$\boldsymbol{G}_i = \boldsymbol{\Delta}_i^H \boldsymbol{H}_i \left(\mathbf{I}_{N_T} + \sum_{u \neq i} \boldsymbol{H}_u^H \boldsymbol{\Delta}_u \boldsymbol{P}_u \boldsymbol{P}_u^H \boldsymbol{\Delta}_u^H \boldsymbol{H}_u \right)^{-1/2}. \tag{24}$$

Considering the covariance matrices for the remaining users as fixed, the derivative with respect to the i-th precoder is

$$\frac{\mathrm{d}g(\boldsymbol{P}_\mathrm{d},\lambda)}{\mathrm{d}\boldsymbol{P}_i^*} = -\boldsymbol{G}_i\boldsymbol{G}_i^\mathrm{H}\left(\mathbf{I}_{N_\mathrm{T}} + \boldsymbol{G}_i^\mathrm{H}\boldsymbol{P}_i\boldsymbol{P}_i^\mathrm{H}\boldsymbol{G}_i\right)^{-1} + \lambda\boldsymbol{P}_i. \quad (25)$$

On the other hand, the derivative with respect to the Lagrangian multiplier is

$$\frac{\mathrm{d}g(\boldsymbol{P}_\mathrm{d},\lambda)}{\mathrm{d}\lambda} = \sum_{u=1}^{U}\|\boldsymbol{P}_u\|_F^2 - P_\mathrm{tx}. \quad (26)$$

Note that this term on λ vanishes as we ensure at each step of the algorithm that the power constraint holds with equality.

APPENDIX B
PROOF OF CONVERGENCE FOR PGA

In this section, we proof the convergence of the proximal gradient algorithm (PGA) in Section IV-B. We first focus on the distance between the unconstrained update at the ℓ-th iteration, $\bar{\boldsymbol{P}}_\mathrm{d}(\ell+1)$, and the update of an optimum of (17), $\boldsymbol{P}_\mathrm{d}^\mathrm{opt}$, which is reduced for appropriate step size $s^{(n)}$, i.e.,

$$\begin{aligned}
&\|\boldsymbol{P}_\mathrm{d}(\ell) - s(\ell)\nabla g(\boldsymbol{P}_\mathrm{d}(\ell)) - \boldsymbol{P}_\mathrm{d}^\mathrm{opt}\|_\mathrm{F}^2 \\
&= \|\boldsymbol{P}_\mathrm{d}(\ell) - \boldsymbol{P}_\mathrm{d}^\mathrm{opt}\|_\mathrm{F}^2 + s^2(\ell)\|\nabla g(\boldsymbol{P}_\mathrm{d}(\ell)) - \nabla g(\boldsymbol{P}_\mathrm{d}^\mathrm{opt})\|_\mathrm{F}^2 \\
&\quad - 2s(\ell)\Re\left\{\mathrm{tr}\left((\boldsymbol{P}_\mathrm{d}(\ell) - \boldsymbol{P}_\mathrm{d}^\mathrm{opt})^\mathrm{H}(\nabla g(\boldsymbol{P}_\mathrm{d}(\ell)) - \nabla g(\boldsymbol{P}_\mathrm{d}^\mathrm{opt}))\right)\right\} \\
&\overset{(a)}{\leq} \|\boldsymbol{P}_\mathrm{d}(\ell) - \boldsymbol{P}_\mathrm{d}^\mathrm{opt}\|_\mathrm{F}^2 + s^2(\ell)\|\nabla g(\boldsymbol{P}_\mathrm{d}(\ell)) - \nabla g(\boldsymbol{P}_\mathrm{d}^\mathrm{opt})\|_\mathrm{F}^2 \\
&\quad - 2s(\ell)\frac{1}{L}\|\nabla g(\boldsymbol{P}_\mathrm{d}(\ell)) - \nabla g(\boldsymbol{P}_\mathrm{d}^\mathrm{opt})\|_\mathrm{F}^2 \\
&\overset{(b)}{\leq} \|\boldsymbol{P}_\mathrm{d}(\ell) - \boldsymbol{P}_\mathrm{d}^\mathrm{opt}\|_\mathrm{F}^2, \quad (27)
\end{aligned}$$

where inequality (a) is obtained as follows. Note that $\nabla g(\boldsymbol{X})$ is differentiable for any $\boldsymbol{X} \in \mathcal{F}$, with $\mathcal{F}$ being the set of feasible solutions to (14). This implies that $\nabla g(\boldsymbol{X})$ is also Lipschitz continuous with parameter $L > 0$, i.e.,

$$\|\nabla g(\boldsymbol{X}) - \nabla g(\boldsymbol{X}^*)\|_\mathrm{F}^2 \leq L\|\boldsymbol{X} - \boldsymbol{X}^*\|_\mathrm{F}^2 \quad \forall \boldsymbol{X}, \boldsymbol{X}^* \in \mathcal{F}. \quad (28)$$

Lipschitz continuity is equivalent to the co-coercivity of a gradient [48], that is,

$$\begin{aligned}
&\Re\left\{\mathrm{tr}\left((\boldsymbol{X} - \boldsymbol{X}^*)^\mathrm{H}(\nabla g(\boldsymbol{X}) - \nabla g(\boldsymbol{X}^*))\right)\right\} \\
&\qquad \geq \frac{1}{L}\|\nabla g(\boldsymbol{X}) - \nabla g(\boldsymbol{X}^*)\|_\mathrm{F}^2 \quad \forall \boldsymbol{X}, \boldsymbol{X}^* \in \mathcal{F}. \quad (29)
\end{aligned}$$

Finally, inequality (b) is obtained if the step size is chosen such that the summation of the second and third terms of the inequality (a) is negative. In other words, $s(\ell)$ must satisfy $0 < s(\ell) < \frac{2}{L}$.

Recall that $\boldsymbol{P}_\mathrm{d}(\ell+1) = \Gamma_{s(\ell)\mu}(\bar{\boldsymbol{P}}_\mathrm{d}(\ell+1))$ and note that the MSO is non-expansive. That is,

$$\|\Gamma(\boldsymbol{X}_1) - \Gamma(\boldsymbol{X}_2)\|_\mathrm{F}^2 \leq \|\boldsymbol{X}_1 - \boldsymbol{X}_2\|_\mathrm{F}^2 \quad (30)$$

for any $\boldsymbol{X}_1, \boldsymbol{X}_2$, as shown in [45, Lemma 1]. Combining the two ideas, we obtain

$$\begin{aligned}
&\|\boldsymbol{P}_\mathrm{d}(\ell+1) - \boldsymbol{P}_\mathrm{d}^\mathrm{opt}\|_\mathrm{F}^2 \\
&\quad = \|\Gamma_{s(\ell)\mu}(\bar{\boldsymbol{P}}_\mathrm{d}(\ell+1)) - \Gamma_{s(\ell)\mu}(\boldsymbol{P}_\mathrm{d}^\mathrm{opt} - s(\ell)\nabla g(\boldsymbol{P}_\mathrm{d}^\mathrm{opt}))\|_\mathrm{F}^2 \\
&\quad \leq \|\bar{\boldsymbol{P}}_\mathrm{d}(\ell+1) - \boldsymbol{P}_\mathrm{d}^\mathrm{opt} + s(\ell)\nabla g(\boldsymbol{P}_\mathrm{d}^\mathrm{opt})\|_\mathrm{F}^2 \\
&\quad \leq \|\boldsymbol{P}_\mathrm{d}(\ell) - \boldsymbol{P}_\mathrm{d}^\mathrm{opt}\|_\mathrm{F}^2. \quad (31)
\end{aligned}$$

Since this result holds for every iteration ℓ, we will obtain a monotonically non-increasing sequence, which eventually leads to a locally optimal solution of (14).

APPENDIX C
PROOF OF CONVERGENCE FOR ITA

In this section we proof the convergence of the iterative trace algorithm (ITA) in Section IV-C. Given the matrices $\boldsymbol{\Delta}_u(\ell)$, $\{\boldsymbol{S}_u(\ell)\}_{u=1}^U$ and $\bar{\boldsymbol{U}}(\ell)$ at the ℓ-th iteration, the constraint in (21) ensures that $\{\boldsymbol{S}_u(\ell+1)\}_{u=1}^U$ fulfills

$$\sum_{u=1}^{U} t_u(\boldsymbol{S}_u(\ell+1), \bar{\boldsymbol{U}}(\ell), \boldsymbol{\Delta}_u(\ell)) \leq \frac{P_\mathrm{tx}}{\alpha(\ell)}. \quad (32)$$

Thus, at iteration $\ell+1$ we obtain a relaxed version of the constraint, i.e.,

$$\begin{aligned}
&\sum_{u=1}^{U} t_u(\boldsymbol{S}_u(\ell+1), \bar{\boldsymbol{U}}(\ell+1), \boldsymbol{\Delta}_u(\ell+1)) \\
&\qquad \leq \sum_{u=1}^{U} t_u(\boldsymbol{S}_u(\ell+1), \bar{\boldsymbol{U}}(\ell), \boldsymbol{\Delta}_u(\ell)) \leq \frac{P_\mathrm{tx}}{\alpha(\ell)}, \quad (33)
\end{aligned}$$

where the inequality comes from the fact that $\bar{\boldsymbol{U}}(\ell+1)$ is the proper truncated basis for $\boldsymbol{\Delta}_u(\ell+1)\boldsymbol{S}_u(\ell+1)\boldsymbol{\Delta}_u^\mathrm{H}(\ell+1)$, and also for $\boldsymbol{\Delta}_u(\ell)\boldsymbol{S}_u(\ell+1)\boldsymbol{\Delta}_u^\mathrm{H}(\ell)$ under the aforementioned assumption $\boldsymbol{\Delta}_u(\ell+1) \approx \boldsymbol{\Delta}_u(\ell)$. This implies that the solution for the iteration ℓ is a feasible solution at the iteration $\ell+1$ and, in addition, the former equality results in less restrictive constraints. Consequently, the objective function increases or remains the same at each iteration. Taking into account that the achievable sum-rate in the downlink for given P_tx is upper bounded, this condition ensures convergence for a fixed $\alpha(\ell)$.

It is, however, desirable to increase the value of $\alpha(\ell)$ at each iteration to obtain a feasible solution. Noting that the inequality in (33) is strict before convergence and defining the update of the step size as $\alpha(\ell+1) = \beta(\ell)\alpha(\ell)$, the parameter $\beta(\ell)$ at each iteration can be determined as

$$\beta(\ell) = \frac{P_\mathrm{tx}}{P_\mathrm{tx} - \alpha(\ell)\delta(\ell)}, \quad (34)$$

with $\delta(\ell) = \sum_{u=1}^{U} t_u(\boldsymbol{S}_u(\ell+1), \bar{\boldsymbol{U}}(\ell+1), \boldsymbol{\Delta}_u(\ell+1)) - t_u(\boldsymbol{S}_u(\ell+1), \bar{\boldsymbol{U}}(\ell), \boldsymbol{\Delta}_u(\ell))$. Thus, (33) also holds for $\alpha(\ell+1) \geq \alpha(\ell)$.

REFERENCES

[1] V. W. S. Wong, R. Schober, D. W. K. Ng, and L.-C. Wang, *Key Technologies for 5G Wireless Systems*. Cambridge, U.K.: Cambridge Univ. Press, 2017.
[2] T. S. Rappaport, S. Sun, R. Mayzus, H. Zhao, Y. Azar, K. Wang, G. N. Wong, J. K. Schulz, M. Samimi, and F. Gutierrez, "Millimeter wave mobile communications for 5G cellular: It will work!," *IEEE Access*, vol. 1, pp. 335–349, 2013.
[3] W. Roh, J.-Y. Seol, J. Park, B. Lee, J. Lee, Y. Kim, J. Cho, K. Cheun, and F. Aryanfar, "Millimeter-wave beamforming as an enabling technology for 5G cellular communications: Theoretical feasibility and prototype results," *IEEE Commun. Mag.*, vol. 52, no. 2, pp. 106–113, Feb. 2014.

[4] F. Boccardi, R. W. Heath, Jr., A. Lozano, T. L. Marzetta, and P. Popovski, "Five disruptive technology directions for 5G," *IEEE Commun. Mag.*, vol. 52, no. 2, pp. 74–80, Feb. 2014.

[5] Z. Pi and F. Khan, "An introduction to millimeter-wave mobile broadband systems," *IEEE Commun. Mag.*, vol. 49, no. 6, pp. 101–107, Jun. 2011.

[6] T. S. Rappaport, R. W. Heath, Jr., R. C. Daniels, and J. N. Murdock, *Millimeter Wave Wireless Communications*. London, U.K.: Pearson, 2015.

[7] E. G. Larsson, O. Edfors, F. Tufvesson, and T. L. Marzetta, "Massive MIMO for next generation wireless systems," *IEEE Commun. Mag.*, vol. 52, no. 2, pp. 186–195, Feb. 2014.

[8] R. Méndez-Rial, C. Rusu, N. González-Prelcic, A. Alkhateeb, and R. W. Heath, Jr., "Hybrid MIMO architectures for millimeter wave communications: Phase shifters or switches?" *IEEE Access*, vol. 4, pp. 247–267, 2016.

[9] R. W. Heath, Jr., N. González-Prelcic, S. Rangan, W. Roh, and A. M. Sayeed, "An overview of signal processing techniques for millimeter wave MIMO systems," *IEEE J. Sel. Topics Signal Process.*, vol. 10, no. 3, pp. 436–453, Apr. 2016.

[10] X. Zhang, A. F. Molisch, and S.-Y. Kung, "Variable-phase-shift-based RF-baseband codesign for MIMO antenna selection," *IEEE Trans. Signal Process.*, vol. 53, no. 11, pp. 4091–4103, Nov. 2005.

[11] A. Alkhateeb, J. Mo, N. Gonzalez-Prelcic, and R. W. Heath, Jr., "MIMO precoding and combining solutions for millimeter-wave systems," *IEEE Commun. Mag.*, vol. 52, no. 12, pp. 122–131, Dec. 2014.

[12] S. Han, I. Chih-Lin, Z. Xu, and C. Rowell, "Large-scale antenna systems with hybrid analog and digital beamforming for millimeter wave 5G," *IEEE Commun. Mag.*, vol. 53, no. 1, pp. 186–194, Jan. 2015.

[13] M. Karabacak, H. Arslan, and G. Mumcu, "Lens antenna subarrays in mmWave hybrid MIMO systems," *IEEE Access*, vol. 8, pp. 216634–216644, 2020.

[14] N. Li, Z. Wei, H. Yang, X. Zhang, and D. Yang, "Hybrid precoding for mmWave massive MIMO systems with partially connected structure," *IEEE Access*, vol. 5, pp. 15142–15151, 2017.

[15] X. Yu, J.-C. Shen, J. Zhang, and K. B. Letaief, "Alternating minimization algorithms for hybrid precoding in millimeter wave MIMO systems," *IEEE J. Sel. Topics Signal Process.*, vol. 10, no. 3, pp. 485–500, Apr. 2016.

[16] J. Zhang, X. Huang, V. Dyadyuk, and Y. Guo, "Massive hybrid antenna array for millimeter-wave cellular communications," *IEEE Wireless Commun.*, vol. 22, no. 1, pp. 79–87, Feb. 2015.

[17] R. A. Stirling-Gallacher and M. S. Rahman, "Multi-user MIMO strategies for a millimeter wave communication system using hybrid beam-forming," in *Proc. IEEE Int. Conf. Commun. (ICC)*, Jun. 2015, pp. 2437–2443.

[18] A. Alkhateeb and R. W. Heath, Jr., "Frequency selective hybrid precoding for limited feedback millimeter wave systems," *IEEE Trans. Commun.*, vol. 64, no. 5, pp. 1801–1818, May 2016.

[19] S. Park, A. Alkhateeb, and R. W. Heath, Jr., "Dynamic subarrays for hybrid precoding in wideband mmWave MIMO systems," 2016, *arXiv:1606.08405*. [Online]. Available: http://arxiv.org/abs/1606.08405

[20] W. Ni and X. Dong, "Hybrid block diagonalization for massive multiuser MIMO systems," *IEEE Trans. Commun.*, vol. 64, no. 1, pp. 201–211, Jan. 2016.

[21] F. Khalid, "Hybrid beamforming for millimeter wave massive multiuser MIMO systems using regularized channel diagonalization," *IEEE Wireless Commun. Lett.*, vol. 8, no. 3, pp. 705–708, Jun. 2019.

[22] J. P. González-Coma and L. Castedo, "Power efficient scheduling and hybrid precoding for time modulated arrays," *IEEE Access*, vol. 8, pp. 21063–21076, 2020.

[23] O. E. Ayach, S. Rajagopal, S. Abu-Surra, Z. Pi, and R. W. Heath, Jr., "Spatially sparse precoding in millimeter wave MIMO systems," *IEEE Trans. Wireless Commun.*, vol. 13, no. 3, pp. 1499–1513, Mar. 2014.

[24] C. Rusu, R. Méndez-Rial, N. González-Prelcic, and R. W. Heath, Jr., "Low complexity hybrid precoding strategies for millimeter wave communication systems," *IEEE Trans. Wireless Commun.*, vol. 15, no. 12, pp. 8380–8393, Dec. 2016.

[25] J. P. González-Coma, J. Rodríguez-Fernández, N. González-Prelcic, L. Castedo, and R. W. Heath, Jr., "Channel estimation and hybrid precoding for frequency selective multiuser mmWave MIMO systems," *IEEE J. Sel. Topics Signal Process.*, vol. 12, no. 2, pp. 353–367, May 2018.

[26] D. H. N. Nguyen, L. B. Le, T. Le-Ngoc, and R. W. Heath, Jr., "Hybrid MMSE precoding and combining designs for mmWave multiuser systems," *IEEE Access*, vol. 5, pp. 19167–19181, 2017.

[27] J. Jin, Y. R. Zheng, W. Chen, and C. Xiao, "Hybrid precoding for millimeter wave MIMO systems: A matrix factorization approach," *IEEE Trans. Wireless Commun.*, vol. 17, no. 5, pp. 3327–3339, May 2018.

[28] Y. Sun, Z. Gao, H. Wang, B. Shim, G. Gui, G. Mao, and F. Adachi, "Principal component analysis-based broadband hybrid precoding for millimeter-wave massive MIMO systems," *IEEE Trans. Wireless Commun.*, vol. 19, no. 10, pp. 6331–6346, Oct. 2020.

[29] F. Sohrabi and W. Yu, "Hybrid digital and analog beamforming design for large-scale antenna arrays," *IEEE J. Sel. Topics Signal Process.*, vol. 10, no. 3, pp. 501–513, Apr. 2016.

[30] M. Kobayashi and G. Caire, "Joint beamforming and scheduling for a multi-antenna downlink with imperfect transmitter channel knowledge," *IEEE J. Sel. Areas Commun.*, vol. 25, no. 7, pp. 1468–1477, Sep. 2007.

[31] T. Yoo and A. Goldsmith, "On the optimality of multiantenna broadcast scheduling using zero-forcing beamforming," *IEEE J. Sel. Areas Commun.*, vol. 24, no. 3, pp. 528–541, Mar. 2006.

[32] S. Vishwanath, N. Jindal, and A. Goldsmith, "Duality, achievable rates, and sum-rate capacity of Gaussian MIMO broadcast channels," *IEEE Trans. Inf. Theory*, vol. 49, no. 10, pp. 2658–2668, Oct. 2003.

[33] T. E. Bogale, L. B. Le, A. Haghighat, and L. Vandendorpe, "On the number of RF chains and phase shifters, and scheduling design with hybrid analog–digital beamforming," *IEEE Trans. Wireless Commun.*, vol. 15, no. 5, pp. 3311–3326, May 2016.

[34] S. Boyd, N. Parikh, E. Chu, B. Peleato, and J. Eckstein, *Distributed Optimization and Statistical Learning via the Alternating Direction Method of Multipliers*. Delft, TheNetherlands: Now Publishers, Jan. 2011.

[35] C. Sun and R. Dai, "A customized ADMM for rank-constrained optimization problems with approximate formulations," in *Proc. IEEE 56th Annu. Conf. Decis. Control (CDC)*, Dec. 2017, pp. 3769–3774.

[36] M. Fazel, H. Hindi, and S. P. Boyd, "A rank minimization heuristic with application to minimum order system approximation," in *Proc. Amer. Control Conf.*, vol. 6, 2001, pp. 4734–4739.

[37] B. Recht, W. Xu, and B. Hassibi, "Necessary and sufficient conditions for success of the nuclear norm heuristic for rank minimization," in *Proc. 47th IEEE Conf. Decis. Control*, Dec. 2008, pp. 3065–3070.

[38] C. Sun and R. Dai, "Rank-constrained optimization and its applications," *Automatica*, vol. 82, pp. 128–136, Aug. 2017.

[39] A. Alkhateeb, O. El Ayach, G. Leus, and R. W. Heath, Jr., "Channel estimation and hybrid precoding for millimeter wave cellular systems," *IEEE J. Sel. Topics Signal Process.*, vol. 8, no. 5, pp. 831–846, Oct. 2014.

[40] N. Jindal, W. Rhee, S. Vishwanath, S. A. Jafar, and A. Goldsmith, "Sum power iterative water-filling for multi-antenna Gaussian broadcast channels," *IEEE Trans. Inf. Theory*, vol. 51, no. 4, pp. 1570–1580, Apr. 2005.

[41] J. P. González-Coma, A. Gründinger, M. Joham, and L. Castedo, "MSE balancing in the MIMO BC: Unequal targets and probabilistic interference constraints," *IEEE Trans. Signal Process.*, vol. 65, no. 12, pp. 3293–3305, Jun. 2017.

[42] C. Eckart and G. Young, "The approximation of one matrix by another of lower rank," *Psychometrika*, vol. 1, no. 3, pp. 211–218, Sep. 1936, doi: 10.1007/BF02288367.

[43] J.-F. Cai, E. J. Candès, and Z. Shen, "A singular value thresholding algorithm for matrix completion," *SIAM J. Optim.*, vol. 20, no. 4, pp. 1956–1982, Jan. 2010.

[44] B. K. Natarajan, "Sparse approximate solutions to linear systems," *SIAM J. Comput.*, vol. 24, no. 2, pp. 227–234, Apr. 1995.

[45] S. Ma, D. Goldfarb, and L. Chen, "Fixed point and Bregman iterative methods for matrix rank minimization," *Math. Program.*, vol. 128, nos. 1–2, pp. 321–353, Jun. 2011.

[46] M. J. Todd, K. C. Toh, and R. H. Tütüncü, "On the Nesterov–Todd direction in semidefinite programming," *SIAM J. Optim.*, vol. 8, no. 3, pp. 769–796, Aug. 1998.

[47] K.-C. Toh, R. Tütüncü, and M. Todd, "On the implementation and usage of SDPT3—A MATLAB software package for semidefinite-quadratic-linear programming, version 4.0," in *Handbook on Semidefinite, Conic and Polynomial Optimization*, vol. 166. Cham, Switzerland: Springer, 2012.

[48] D. L. Zhu and P. Marcotte, "Co-coercivity and its role in the convergence of iterative schemes for solving variational inequalities," *SIAM J. Optim.*, vol. 6, no. 3, pp. 714–726, Aug. 1996.

JOSÉ P. GONZÁLEZ-COMA (Member, IEEE) was born in Marín, Spain. He received the degree in computer engineering and the Ph.D. degree from the University of A Coruña, Spain, in 2009 and 2015, respectively. In 2009, he was with the Group of Electronic Technology and Communications (GTEC), University of A Coruña, where he received the FPI Grant from the Ministerio de Ciencia e Innovación, in 2011. He was a Visiting Researcher with the Associate Institute for Signal Processing, Technische Universität München, Germany, in 2012, and also with the Signal Processing in Communications Group (UVIGO), Spain, in 2017. Since 2020, he has been with the Defense University Center, Spanish Naval Academy. His current research interests include channel estimation and precoding in massive multi-in multi-out systems, and millimeter-wave communications.

ÓSCAR FRESNEDO (Member, IEEE) received the degree in computer engineering and the Ph.D. degree in computer engineering from the University of A Coruña, Spain, in 2007 and 2014, respectively. Since 2007, he has been with the Group of Electronic Technology and Communications (GTEC), Department of Electronics and Systems, University of A Coruña, where he had the benefit of a FPI scholarship granted by the Spanish Government, from 2008 to 2012. He has published 13 articles in international technical journals and more than 30 papers in relevant international conferences and workshops in the area of communications and signal processing. He has participated as a research member in more than ten research projects and contracts granted by regional, national, and European administrations. His current research interests include the design of coding schemes, analog joint source-channel coding, multiuser communications, and image processing. He received the Best Student Paper Award at the 14th IEEE International Workshop on Signal Processing Advances in Wireless Communications (SPAWC), Darmstadt, in 2013.

LUIS CASTEDO (Senior Member, IEEE) received the Ph.D. degree in telecommunications engineering from the Technical University of Madrid, Spain, in 1993. Since 1994, he has been a Faculty Member with the Department of Computer Engineering, University of A Coruña (UDC), Spain, where he became a Professor in 2001 and acted as the Chairman from 2003 to 2009. He had previously held several research appointments at the University of Southern California (USC) and École supérieure d'électricité (SUPELEC). From 2014 to 2018, he was a Manager of the Communications and Electronic Technologies (TEC) program in the State Research Agency of Spain. He has also been the principal researcher of more than 50 research projects funded by public organisms and private companies. He has coauthored more than 300 papers in peer-reviewed international journals and conferences. His research interests include signal processing for wireless communications and the prototyping of digital communication equipments. His articles have received three Best Student Paper Awards at the IEEE/ITG Workshop on Smart Antennas, in 2007, at the IEEE International Workshop on Signal Processing Advances in Wireless Communications, in 2013, and at the IEEE International Conference on Internet of Things (iThings), in 2017. He has been a General Co-Chair of the 8th IEEE Sensor Array and Multichannel Signal Processing Workshop, in 2014, and the 27th European Signal Processing Conference, in 2019.